Structural Engineering and Mechanics, Vol. 30, No. 6 (2008) 763-785
DOI: http://dx.doi.org/10.12989/sem.2008.30.6.763

Nonlinear inelastic analysis of steel-concrete composite beam-columns using the stability functions

Jung-Woong Park and Seung-Eock Kim†

Department of Civil and Environmental Engineering, Sejong University, 98 Gunja-dong, Gwangjin-gu, Seoul, 143-747, Korea

(Received August 26, 2008, Accepted November 10, 2008)

Abstract. In this study, a flexibility-based finite element method considering geometric and material nonlinearities is developed for analyzing steel-concrete frame structures. The stability functions obtained from the exact buckling solution of the beam-column subjected to end moments are used to accurately capture the second-order effects. The proposed method uses the force interpolation functions, including a moment magnification due to the axial force and lateral displacement. Thus, only one element per a physical member can account for the interaction between the bending moment and the axial force in a rational way. The proposed method applies the Newton method based on the load control and uses the secant stiffness method, which is computationally both efficient and stable. According to the evaluation result of this study, the proposed method consistently well predicts the nonlinear inelastic behavior of steel-concrete composite frames and gives good efficiency.

Keywords: nonlinear analysis; stability functions; beam-column element; composite structures; concrete-filled steel tube.

1. Introduction

Recently, researchers have focused attention on force-based and mixed formulations that permit more accurate representation of the force distribution along the element. Since there are no displacement interpolation functions to relate the section deformations to nodal displacements, it is still challenging to implement the flexibility-based methods for nonlinear problems in the context of a finite element program. Ciampi and Carlesimo (1986) proposed the consistent formulation of force-based elements. Their procedure was improved by Taucer, Spacone, and Filippou (1991), and Spacone, Filippou, and Taucer (1996) to develop a force-based fiber frame element for nonlinear analysis of reinforced concrete structures. Spacone, Ciampi, and Fillipou (1996) proposed the general formulation of a mixed approach, which points the way to the consistent numerical implementation of the element state determination. Ayoub and Filippou (2000) presented an inelastic beam element for the analysis of steel-concrete girders with partial composite using a two-field mixed formulation with independent approximation of internal forces and transverse displacements.

† Professor, Corresponding author, E-mail: sekim@sejong.ac.kr

Ayoub (2003) extends the mixed formulation to analyze inelastic beams on foundations, where both the beam and foundation are assumed to be inelastic. Alemdar and White (2005) developed both a first order flexibility-based model within a corotational approach and a two-field mixed model. Hjelmstad and Taciroglu (2002) compared the variational approaches with the so-called nonlinear flexibility methods that have recently been reported in the literature, and conclude that these approaches, while certainly having merit, are not variationally consistent.

Although the geometric second-order effects are important in the frame structures and sometimes they are quite plain, most of the force-based methods do not consider the geometric second-order effects. The structural analysis including the second-order effects is further complicated by the fact that the resulting equilibrium equations are differential equations instead of the usual algebraic equations. For a slender column, buckling may occur when all fibers of the cross-section are still elastic. Thus, the Euler load will govern the load-carrying capacity of the column. For a short column, material yielding of the fibers in the cross-section usually occurs before buckling takes place, so the yielding force of the section will govern the limit state of the column. In reality of practice, some of the fibers of the cross-section may yield while some fibers still remain elastic, and the failure may be more accurately described as combined buckling of the column and material yielding of the section.

In this study, a flexibility-based finite element method considering geometric second-order effects and material inelasticity is developed to improve the common flexibility-based methods which have been proposed up to now. The stability functions obtained from the exact buckling solution of the beam-column subjected to end moments are used to accurately capture the second-order effects. The proposed method uses the force interpolation functions including a moment magnification due to the axial force and lateral displacement. Thus, only one element per a physical member can account for the interaction between the bending moment and the axial force in a rational way. To verify the accuracy and computational efficiency of the proposed method, the results are compared with those obtained from the experiments, theoretical equations, and OpenSees (2008), which is a software framework for research in performance-based earthquake engineering at the Pacific Earthquake Engineering Research Center. The details of the proposed method are now presented.

2. Beam-column element formulation

2.1 The principle of virtual work

The principle of virtual work states that external virtual work is simply the product of the displacements and their applied virtual forces, and internal virtual work is expressed by the product of strain resultants and their virtual stress resultants integrated over the cross-section.

$$\delta\mathbf{F}(x)^T\mathbf{d}(x) = \int \delta\mathbf{M}(x)^T\boldsymbol{\varphi}(x)dx \tag{1}$$

where

$$\mathbf{d} = \{\theta_{1z} \quad \theta_{2z} \quad \theta_{1y} \quad \theta_{2y} \quad d_x\}^T \tag{2}$$

$$\mathbf{F} = \{M_{1z} \quad M_{2z} \quad M_{1y} \quad M_{2y} \quad P\}^T \tag{3}$$

$$\boldsymbol{\varphi} = \{\phi_z \quad \phi_y \quad \varepsilon_x\}^T \tag{4}$$

$$\mathbf{M} = \{M_z \quad M_y \quad P\}^T \tag{5}$$

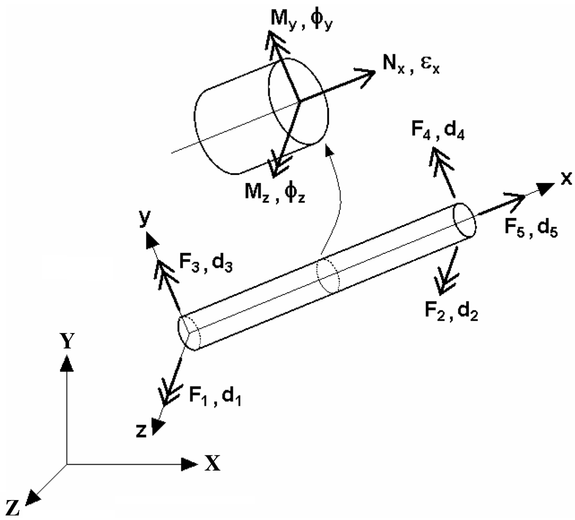

Fig. 1 Forces and deformation at the element and section levels

Fig. 1 shows that the element deformations of Eq. (2) and element end forces of Eq. (3). One element has five degrees of freedom: an axial extension and two rotations per each node. Element forces of Eq. (3) indicate the corresponding axial force and bending moments. Fig. 1 also shows the section deformations of Eq. (4) and section forces of Eq. (5). Section deformations are three strain resultants: an axial strain and two curvatures with respect to local z and y axes. Section forces include the compressive axial force and two sectional bending moments. All of the fields given in Eqs. (2) to (5) are functions of the axial coordinate x, which is measured from the left end of the beam, as shown in Fig. 1.

2.2 Displacement-based and flexibility-based formulations

In the displacement-based formulation (usually called the stiffness method), the displacement fields are approximated by displacement interpolation functions as

$$\varphi = \mathbf{A}(x)\mathbf{d} \tag{6}$$

where $\mathbf{A}(x)$ contains the derivatives of the displacement interpolation functions as

$$\mathbf{A}(x) = \begin{bmatrix} 0 & 0 & 0 & N^{v}_{1,xx} & N^{\theta}_{1,xx} & 0 & 0 & 0 & N^{v}_{2,xx} & N^{\theta}_{2,xx} \\ 0 & N^{v}_{1,xx} & N^{\theta}_{1,xx} & 0 & 0 & 0 & N^{v}_{2,xx} & N^{\theta}_{2,xx} & 0 & 0 \\ N^{u}_{1,x} & 0 & 0 & 0 & 0 & N^{u}_{2,x} & 0 & 0 & 0 & 0 \end{bmatrix} \tag{7}$$

where

$$N^{v}_{1} = 2\frac{x^3}{L^3} - 3\frac{x^2}{L^2} + 1; \quad N^{v}_{2} = 3\frac{x^2}{L^2} - 2\frac{x^3}{L^3} \tag{8}$$

$$N^{\theta}_{1} = \frac{x^3}{L^2} - 2\frac{x^2}{L} + x; \quad N^{\theta}_{2} = \frac{x^3}{L^2} - \frac{x^2}{L} \tag{9}$$

$$N_1^u = 1 - \frac{x}{L};\ N_2^u = \frac{x}{L} \tag{10}$$

The main shortcoming of the stiffness method is that the predefined displacement interpolation functions do not correspond to the exact solution of the beam problem except for in special cases. Since the assumption of cubic interpolation functions gives a linear curvature distribution along the element, a highly refined mesh is needed to accurately capture the response of the regions with highly nonlinear curvature distribution. Also, equilibrium is satisfied only in an integral sense over the element, but not locally at each section along the beam.

The principal of virtual work and Taylor's series expansion give a linear algebraic problem as follows

$$\mathbf{F} - \int \mathbf{A}^T \mathbf{M}_R dx = \int \mathbf{A}^T \mathbf{k} \mathbf{A} dx \Delta \mathbf{d} \tag{11}$$

where $\mathbf{M}_R$ is the section resisting force vector, and $\mathbf{k}$ is the section stiffness matrix. The left hand side term in Eq. (11) is the unbalance force given as the difference between the external element force and the element resisting force, and is a function of the deformed configuration. The solution of this nonlinear problem by Newton's method involves iteratively solving the system of Eq. (11).

In the force-based formulation (usually called the flexibility method), the force fields are expressed as a function of the element nodal forces

$$\mathbf{M} = \mathbf{B}(x)\mathbf{F} \tag{12}$$

where $\mathbf{B}(x)$ is the force interpolation functions that enforce a linear bending moment distribution along the element and a moment magnification due to the axial force and lateral displacement:

$$\mathbf{B}(x) = \begin{bmatrix} \left(\frac{x}{L} - 1\right) & \left(\frac{x}{L}\right) & 0 & 0 & -\delta_y \\ 0 & 0 & \left(\frac{x}{L} - 1\right) & \left(\frac{x}{L}\right) & -\delta_z \\ 0 & 0 & 0 & 0 & 1 \end{bmatrix} \tag{13}$$

where δ_y and δ_z are the lateral displacements for the local y and z axes, respectively. The terms of δ_y and δ_z in Eq. (13) are newly added ones in this study. Since the curvature can be approximated by the second derivative of the lateral displacement, δ_y and δ_z are obtained from solving the differential equations as (Chen and Lui 1987)

$$\delta_y = -\frac{M_{1z}}{EI_z k_z^2}\left[\frac{\cos k_z L}{\sin k_z L}\sin k_z x - \cos k_z x - \frac{x}{L} + 1\right] - \frac{M_{2z}}{EI_z k_z^2}\left[\frac{1}{\sin k_z L}\sin k_z x - \frac{x}{L}\right] \tag{14}$$

$$\delta_z = \frac{M_{1y}}{EIk_y^2}\left[\frac{\cos k_y L}{\sin k_y L}\sin k_y x - \cos k_y x - \frac{x}{L} + 1\right] - \frac{M_{2y}}{EIk_y^2}\left[\frac{1}{\sin k_y L}\sin k_y x - \frac{x}{L}\right] \tag{15}$$

where $k_z^2 = P/EI_z$ and $k_y^2 = P/EI_y$.

Since the section flexibility relates the strain resultants to the section moments, and the element stiffness relates the element end forces to the element end displacements, the strain resultants are given as

$$\varphi = \mathbf{f}\mathbf{B}(x)\mathbf{K}\mathbf{d} \tag{16}$$

where $\mathbf{f}$ is the section flexibility matrix and $\mathbf{K}$ is the element stiffness matrix. Comparing Eq. (6) and Eq. (16) expresses the displacement interpolation function $\mathbf{A}(x)$ as

$$\mathbf{A}(x) = \mathbf{f}\mathbf{B}(x)\mathbf{K} \tag{17}$$

From Eq. (17), $\mathbf{A}(x)$ and $\mathbf{B}(x)$ are dependent upon each other, and this property is shown in general flexibility-based formulations.

The main advantage of the flexibility methods is that force interpolation functions inside the element are better suited to describe the nonlinear behavior of structural members. In the absence of element loads, a linear bending moment distribution along the element satisfies equilibrium in a strict sense. Accordingly, it provides the benefit of computing the exact element flexibility matrix.

2.3 Element stiffness accounting for $P-\delta$ effect

To capture the effect of the axial force acting through the lateral displacement of the beam-column element relative to its chord ($P-\delta$ effect), the slope-deflection equations for a beam-column were presented by Chen and Lui (1987). Generally only one element per a physical member can accurately account for the $P-\delta$ effect. The element end forces and the element end displacements are related as

$$\begin{Bmatrix} M_{1z} \\ M_{2z} \\ M_{1y} \\ M_{2y} \\ P \end{Bmatrix} = \frac{1}{L}\begin{bmatrix} EI_z s_{zii} & EI_z s_{zij} & 0 & 0 & 0 \\ EI_z s_{zij} & EI_z s_{ii} & 0 & 0 & 0 \\ 0 & 0 & EI_y s_{yii} & EI_y s_{yij} & 0 \\ 0 & 0 & EI_y s_{yij} & EI_y s_{yii} & 0 \\ 0 & 0 & 0 & 0 & EA \end{bmatrix}\begin{Bmatrix} \theta_{1z} \\ \theta_{2z} \\ \theta_{1y} \\ \theta_{2y} \\ d \end{Bmatrix} \tag{18}$$

where s_{zii}, s_{zij}, s_{yii} and s_{yij} are the stability functions with respect to the local z and y axes, and are given as

$$s_{nii} = \frac{k_nL\sin k_nL - (k_nL)^2\cos k_nL}{2-2\cos k_nL - k_n\sin k_nL} \tag{19a}$$

$$s_{nij} = \frac{(k_nL)^2 - k_nL\sin k_nL}{2-2\cos k_nL - k_n\sin k_nL} \tag{19b}$$

where the subscript n represents for z or y The three-dimensional slope-deflection equations for a beam-column that is not subjected to transverse loadings and relative joint translation can be expressed in symbolic form as

$$\mathbf{M} = \mathbf{K}_e\mathbf{d} \tag{20}$$

For members subjected to an axial force that is tensile rather than compressive, the stability functions in Eq. (19) are redefined as

$$s_{nii} = \frac{(k_nL)^2\cosh k_nL - k_nL\sinh k_nL}{2-2\cos k_nL + k_nL\sin k_nL} \tag{21a}$$

$$s_{nij} = \frac{k_nL\sinh k_nL - (k_nL)^2}{2-2\cosh k_nL + k_nL\sinh k_nL} \tag{21b}$$

For a pinned-ended perfectly straight column subjected to a compressive axial force, the theoretical load-deflection curve of the column bifurcates into stable and unstable equilibrium branches at the point when s_{ii} is equal to s_{ij}.

2.4 Element stiffness accounting for $P-\Delta$ effect

The $P-\Delta$ effect is the effect of member forces acting through the relative transverse displacement of the member ends. If the member is permitted to sway, an additional axial and shear force will be induced in the member. We can relate this additional axial and shear force due to a member sway to the member end displacements as

$$\{\mathbf{F}_L\}_s = [\mathbf{K}]_s\{\mathbf{d}_L\} \tag{22}$$

where $\{\mathbf{F}_L\}_s$ and $\{\mathbf{d}_L\}$ are end force and displacement vectors, and $\{\mathbf{K}\}_s$ is the element stiffness matrix given as (Kim *et al.* 2006)

$$[\mathbf{K}_s]_{10\times 10} = \begin{bmatrix} [\mathbf{K}_s] & -[\mathbf{K}_s] \\ -[\mathbf{K}_s]^T & [\mathbf{K}_s] \end{bmatrix} \tag{23}$$

where

$$[\mathbf{K}_s]_{10\times 10} = \begin{bmatrix} 0 & a & -b & 0 & 0 \\ a & c & 0 & 0 & 0 \\ -b & 0 & c & 0 & 0 \\ 0 & 0 & 0 & 0 & 0 \\ 0 & 0 & 0 & 0 & 0 \end{bmatrix} \tag{24}$$

and

$$a = \frac{M_{1z}+M_{2z}}{L^2}; \quad b = \frac{M_{1y}+M_{2y}}{L^2}; \quad c = \frac{P}{L} \tag{25}$$

Using equilibrium and kinematic relations, the transformation matrix is given as

$$[\mathbf{T}]_R = \begin{bmatrix} 0 & 1/L & 0 & 0 & 1 & 0 & -1/L & 0 & 0 & 0 \\ 0 & 1/L & 0 & 0 & 0 & 0 & -1/L & 0 & 0 & 1 \\ 0 & 0 & -1/L & 1 & 0 & 0 & 0 & 1/L & 0 & 0 \\ 0 & 0 & -1/L & 0 & 0 & 0 & 0 & 1/L & 1 & 0 \\ -1 & 0 & 0 & 0 & 0 & 1 & 0 & 0 & 0 & 0 \end{bmatrix} \tag{26}$$

The total element stiffness matrix is now given by

$$[\mathbf{K}]_t = [\mathbf{T}_R]^T[\mathbf{K}_e][\mathbf{T}_R] + [\mathbf{K}]_s \tag{27}$$

The use of Eq. (27) requires iterative solution techniques since the section forces in a member change during the iteration process. Excessive $P-\Delta$ effects will eventually introduce singularities into the solution, indicating physical structural instability. Such behavior is clearly indicative of a poorly designed structure that is in a need of additional stiffness.

2.5 Fiber model

The resultant force and moment can be calculated by integrating the tractions over the cross-sectional area, as shown in Fig. 2 (Hjelmstad 1997),

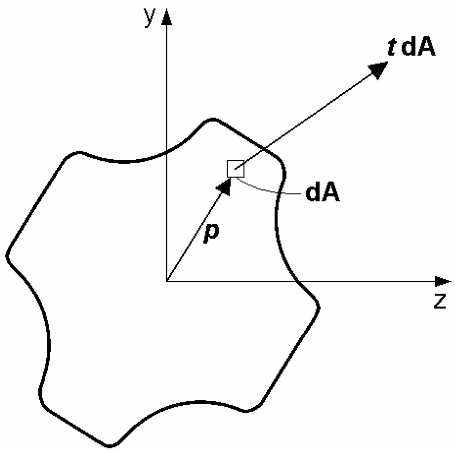

Fig. 2 Traction vector acting on a plane

$$\mathbf{N}(x) = \int \mathbf{t}(x)dA \tag{28}$$

$$\mathbf{M}(x) = \int \mathbf{p}(z,y) \times \mathbf{t}(x)dA \tag{29}$$

where $\mathbf{t}(x)$ is traction vector acting on a plane perpendicular to the longitudinal axis and $\mathbf{p}(z,y)$ is the position vector of this traction vector in the plane. Using a one-dimensional version of the Cauchy formula relating stress to tractions, Eqs. (28) and (29) can be rewritten as

$$N = \int (\varepsilon_0 - y\phi_z + z\phi_y)EdA \tag{30}$$

$$M_z = \int -y(\varepsilon_0 - y\phi_z + z\phi_y)EdA \tag{31}$$

$$M_y = \int z(\varepsilon_0 - y\phi_z + z\phi_y)EdA \tag{32}$$

In the fiber model, the element is subdivided into a number of longitudinal fibers. The center coordinates in the local $z - y$ reference system, and the fiber areas are used in formulating the element stiffness matrix. The constitutive relation of the section is now expressed from the uniaxial response of the fibers

$$\mathbf{k} = \begin{bmatrix} \sum_{i=1}^{n} E_iA_iy_i^2 & \sum_{i=1}^{n} E_iA_i(-y_i)z_i & \sum_{i=1}^{n} E_iA_i(-y_i) \\ \sum_{i=1}^{n} E_iA_i(-y_i)z_i & \sum_{i=1}^{n} E_iA_iz_i^2 & \sum_{i=1}^{n} E_iA_iz_i \\ \sum_{i=1}^{n} E_iA_i(-y_i) & \sum_{i=1}^{n} E_iA_iz_i & \sum_{i=1}^{n} E_iA_i \end{bmatrix} \tag{33}$$

The **M** and φ are duals of each other, in the sense that they are meant to represent exactly the same constitutive relation. In a flexibility-based method, the section deformations is determined from the given section forces.

3. Constitutive relationships

Concrete-filled steel tubes (CFT) are becoming increasingly popular in recent decades due to their excellent performance such as high ductility and improved strength without increasing the size of the column. Also, using CFT members makes the construction easier by eliminating the arrangement of formwork and reinforcement. When CFT members are subjected to compressive strains, both the steel tube and the concrete core experience a lateral expansion. The lateral expansion of concrete core gradually becomes greater than the steel tube due to the change of the Poisson ratio of the concrete. At this stage, a radial pressure develops between the two media, and the steel tube restraints the concrete core to expand laterally. The effect of confinement on the concrete core primarily depends on the lateral pressure provided by the steel tube. Susantha et al. (2001) has performed extensive parametric analyses to propose mathematical equations for the average maximum lateral pressure, f_{rp} in the box and octagonal shaped CFT columns. For box shaped CFT column, f_{rp} is as follows:

$$f_{rp} = -6.5R\frac{(f_c')^{1.46}}{f_y} + 0.12(f_c')^{1.03} \tag{34}$$

$$R = \frac{b}{t}\sqrt{\frac{12(1-v^2)}{4\pi^2}}\sqrt{\frac{f_y}{E_s}} \tag{35}$$

where f_{rp} is the lateral confining pressure, R is the width-to-thickness ratio parameter, b is the width of the section, t is the thickness of the steel tube, and v is the Poisson ratio of the steel. The compressive strength of confined concrete is given as

$$f_{cc} = f_c' + 4.0f_{rp} = \beta f_c' \tag{36}$$

where β is the strength enhancement factor. The Fig. 3 shows the strength enhancement factors with respect to Rf_c'/f_y ratios that depend on the geometry and material properties.

The compressive stress-strain curve for the confined concrete is defined for the pre-peak region as

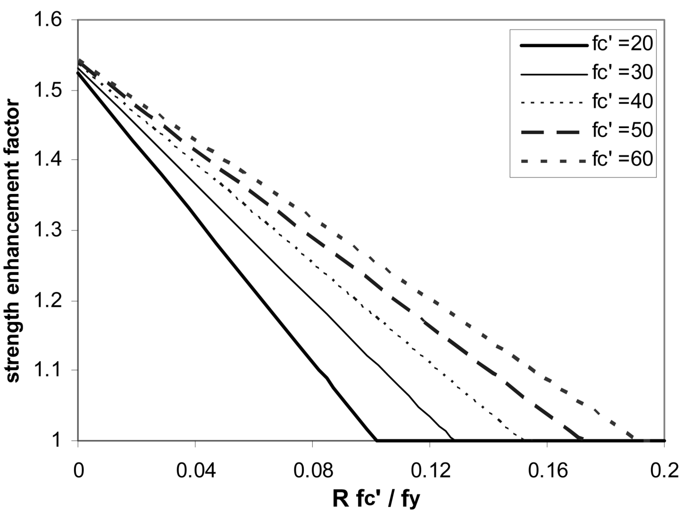

Fig. 3 Strength enhancement factor

(Popovics 1973; Mander *et al.* 1988)

$$f_c = f_{cc}\frac{(\varepsilon/\varepsilon_{cc})r}{r-1+(\varepsilon/\varepsilon_{cc})^r} \tag{37}$$

$$r = \frac{E_c}{E_c-(f_{cc}/\varepsilon_{cc})} \tag{38}$$

$$\varepsilon_{cc} = \varepsilon_0\left[1+5\left(\frac{f_{cc}}{f_c'}-1\right)\right] \tag{39}$$

where ε_{cc} is the compressive strain corresponding to the peak strength f_{cc}. The slope, Z of the post-peak behavior proposed by Susantha *et al.* (2001) is expressed as

$$Z = \begin{cases} 0 & \text{for } R\dfrac{f_c'}{f_y} \le 0.0039 \\ 23,400R\dfrac{f_c'}{f_y}-91.26 & \text{for } R\dfrac{f_c'}{f_y} > 0.0039 \end{cases} \tag{40}$$

$$\varepsilon_{cu} = \begin{cases} 0.04 & \text{for } R\dfrac{f_c'}{f_y} \le 0.042 \\ 14.5\left(R\dfrac{f_c'}{f_y}\right)-2.4R\dfrac{f_c'}{f_y}+0.116 & \text{for } 0.042 < R\dfrac{f_c'}{f_y} < 0.073 \\ 0.018 & \text{for } R\dfrac{f_c'}{f_y} > 0.073 \end{cases} \tag{41}$$

According to the Eqs. (40) and (41), thick-walled steel tubes with low-strength filled-in concrete provide higher ductility capacity than the thin-walled tubes with high-strength filled-in concrete. For low B/t ratios, local buckling usually takes place in the post-peak region of the load-deflection curve of the column (Tort and Hajjar 2004). This type of response is ductile and it can be ensured by specifying a maximum allowable B/t value according to the AISC Specification (2005).

Concrete strength between cracks is generally modeled to reduce gradually after a crack forms based on tension stiffening. In this study, a linear tension softening model is applied. The compressive and tensile stress-strain relationships of unconfined and confined concrete are shown in Fig. 4. The stress-strain relationship for a reinforcement bar is assumed to be tri-linear. It consists of an initial linear elastic region, a yield plateau, and a linear strain-hardening phase.

4. Current design codes

Design methods for CFT columns are available in various major design codes such as the AISC (2005), the ACI 318-05 (2005), the Architectural Institute of Japan (1997), the European Code EC 4 (2004). The design methods of AISC and ACI codes are briefly summarized below.

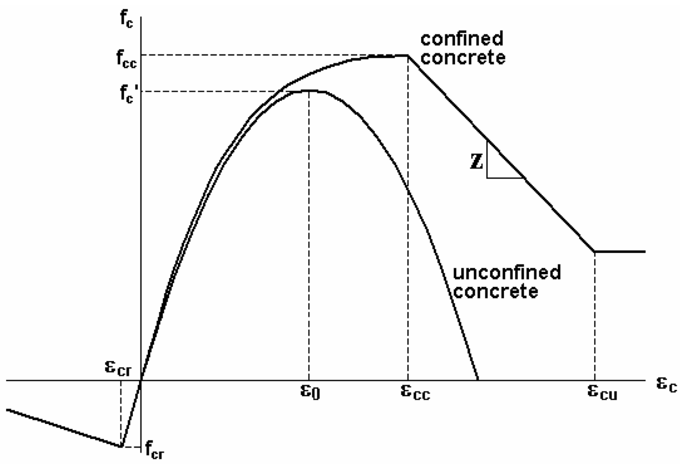

Fig. 4 Stress-strain relationships of concrete

4.1 American Institute of Steel Construction (2005)

The 2005 AISC (2005) now uses a cross-sectional strength approach for column design consistent with that used in reinforced concrete design (ACI 2005). The available axial strength, including the effects of buckling, and the available flexural strength can be calculated using either the plastic stress distribution method or the strain-compatibility method. The simplified approaches can be applied to take advantage of strength determination using a limited number of cases and interpolation for all other cases on the points of interaction diagram. The nominal compressive strength of rectangular CFT column is given as

$$P_n = P_0\left[0.658^{\left(\frac{P_0}{P_e}\right)}\right] \quad \text{for} \quad P_e \ge 0.44P_0 \tag{42}$$

$$P_n = 0.877P_e \quad \text{for} \quad P_e < 0.44P_0 \tag{43}$$

where

$$P_0 = A_s f_y + 0.85 A_c f_c' \tag{44}$$

$$P_e = \pi^2 EI_{eff}/(KL)^2 \tag{45}$$

where is the effective stiffness of composite section given as

$$EI_{eff} = E_s I_s + C_3 E_c I_c \tag{46}$$

$$C_3 = 0.6 + 2\left(\frac{A_s}{A_c + A_s}\right) \le 0.9 \tag{47}$$

The maximum *B*/*t* ratio for a rectangular CFT column shall be equal to $2.26\sqrt{E_s/f_y}$.

4.2 American Concrete Institute (2005)

The design concept of a CFT column is essentially the same as that of an ordinary reinforced concrete column. To apply strain compatibility method, a continuous steel tube in a CFT is converted into equivalent reinforcing bars around the filled-in concrete. It assumes that the concrete has reached its crushing strength in compression at a strain of 0.003 with a rectangular stress block. However, the ultimate stress is taken as f_c' instead of $0.85f_c'$ to reflect that concrete inside tubes does not split with providing high ductility and improved strength.

Slenderness effect should be considered in the following cases

$$\frac{kl_u}{r} > 22 \quad \text{for non-sway case} \tag{48}$$

$$\frac{kl_u}{r} > 34 - 12\frac{M_1}{M_2} \quad \text{for sway case} \tag{49}$$

where kl_u is the effective length, M_1 and M_2 are smaller and larger end moments, respectively, and r is a radius of gyration. The moment amplified for the effects of member curvature is given as

$$M_c = \frac{C_m}{1 - P/(0.75P_c)} M_0 \tag{50}$$

$$C_m = 0.6 + 0.4\frac{M_1}{M_2} \tag{51}$$

where C_m is a correction factor relating the actual moment diagram to an equivalent uniform moment diagram, and M_1/M_2 is positive if the column is bent in single curvature, and negative if the member is bent in double curvature. The beam-column analysis using strain compatibility method can be readily implemented in a spreadsheet.

5. Numerical examples

To verify the accuracy of the proposed method, the 116 rectangular CFT columns tested to failure, five end-restrained steel columns, and a 3-dimensional CFT frame structure are analyzed. Failure strengths of the 116 rectangular CFT columns are predicted by the AISC, ACI 318-05, and the proposed method, and the results are compared with those obtained from the experiments of the following 6 investigations: Tomii and Sakino (1979), Liu (2004), Liu, Gho, and Yuan (2003), Lue, Liu, and Yen (2007), Liu (2005), and Liu (2006). The details of the test specimens and strength ratios (P_{test}/P_n or M_{test}/M_n) are given for each group of test results in Tables 1-6 and collectively in Fig. 5. A brief description of each testing program from which the test results were extracted is presented below.

Tomii and Sakino (1979) tested 36 rectangular CFT specimens which are composed of 8 concentrically loaded columns and 28 columns subjected to axial load and bending moments. After the constant axial load was applied, a monotonic increasing moment was applied to the specimens. The rotation, deflections and strains were recorded between load applications. The deflections were held constant during this time. This resulted in a decrease of bending moment due to creep, but since the readings were performed relatively quickly, it was assumed that the creep effects on the measurements were probably unimportant. They reported that the magnitude of constant axial load and B/t ratio had a significant effect on an inelastic behavior, especially on the descending branch of the moment-curvature relationships.

Table 1 Analysis results for test data 1 (Tomii and Sakino 1979)

Specimen	B, H (mm)	t (mm)	L (mm)	f_c' (MPa)	f_y (MPa)	P_{test} (kN)	M_{test} (kN·m)	P_{test}/P_n or M_{test}/M_n		
								ACI 05	AISC 05	Authors
I-A	100	2.29	300	31.97	194.2	497.2	0	1.07	1.18	1.02
I-B	100	2.29	300	31.97	194.2	498.2	0	1.07	1.19	1.02
II-A	100	2.2	300	21.38	339.3	510.9	0	1.05	1.12	0.96
II-B	100	2.2	300	21.38	339.3	510.0	0	1.05	1.12	0.96
III-A	100	2.99	300	20.59	288.3	528.6	0	1.02	1.08	0.93
III-B	100	2.99	300	20.59	288.3	527.6	0	1.02	1.08	0.93
IV-A	100	4.25	300	19.81	284.4	666.9	0	1.06	1.11	0.97
IV-B	100	4.25	300	19.81	284.4	665.9	0	1.06	1.11	0.97
I-0	100	2.29	300	24.03	194.2	0	7.2	0.96	0.96	1.00
I-1	100	2.29	300	38.25	194.2	76.5	10.2	1.08	1.08	1.12
I-2	100	2.29	300	38.25	194.2	157.9	11.2	1.09	1.09	1.09
I-3	100	2.29	300	38.25	194.2	191.2	11.2	1.09	1.09	1.08
I-5	100	2.29	300	38.25	194.2	267.7	11.5	1.25	1.25	1.15
I-6	100	2.29	300	36.68	194.2	330.5	8.9	1.28	1.28	1.10
I-6'	100	2.29	300	36.68	194.2	330.5	8.2	1.18	1.18	1.06
II-0	100	2.27	300	21.57	305	0	11.0	0.99	0.99	1.05
II-1	100	2.27	300	21.57	305	46.1	12.4	1.05	1.05	1.09
II-2	100	2.2	300	21.57	339.3	92.2	12.9	1.03	1.03	1.01
II-3	100	2.2	300	21.57	339.3	138.3	12.7	1.03	1.03	0.98
II-4	100	2.22	300	21.57	289.3	184.4	11.8	1.17	1.17	1.03
II-5	100	2.22	300	21.57	289.3	231.4	10.7	1.25	1.25	1.02
II-6	100	2.22	300	21.57	289.3	277.5	9.1	1.31	1.31	1.01
III-0	100	2.98	300	20.59	289.3	0	14.0	1.05	1.05	1.10
III-1	100	2.98	300	20.59	289.3	51.0	14.6	1.06	1.06	1.06
III-2	100	2.98	300	20.59	289.3	102.0	15.2	1.1	1.1	1.06
III-3	100	2.99	300	20.59	288.3	153.0	14.5	1.09	1.09	1.01
III-4	100	2.99	300	20.59	288.3	204.0	13.3	1.11	1.11	0.97
III-5	100	2.99	300	20.59	288.3	255.0	12.5	1.21	1.21	0.98
III-6	100	2.99	300	20.59	288.3	306.0	10.8	1.26	1.26	0.98
IV-0	100	4.25	300	18.63	284.4	0	18.3	1.04	1.04	1.06
IV-1	100	4.25	300	18.63	284.4	61.8	19.0	1.06	1.06	1.05
IV-2	100	4.25	300	18.63	284.4	123.6	18.8	1.06	1.06	1.02
IV-3	100	4.25	300	18.63	285.4	185.4	18.2	1.08	1.08	1.00
IV-4	100	4.25	300	19.81	285.4	251.1	17.4	1.16	1.16	0.99
IV-5	100	4.25	300	19.81	285.4	313.8	15.8	1.24	1.24	0.99
IV-6	100	4.26	300	19.81	288.3	375.6	14.0	1.31	1.31	1.00
Average								1.11	1.13	1.02
Coefficient of variation								0.08	0.08	0.05

Table 2 Analysis results for test data 2 (Liu 2004)

Specimen	B (mm)	H (mm)	t (mm)	L (mm)	f_c' (MPa)	f_y (MPa)	P_{test} (kN)	M_{test} (kN·m)	P_{test}/P_n or M_{test}/M_n		
									ACI 05	AISC 05	Authors
E01	150	150	4.18	870	60.8	550	1678	50.3	1.09	1.09	0.95
E02	150	150	4.18	870	72.1	550	1850	55.5	1.13	1.13	0.97
E03	150	150	4.18	2170	60.8	550	1330	39.9	1.21	1.21	0.92
E04	150	150	4.18	2170	72.1	550	1020	61.2	1.22	1.22	0.98
E05	120	180	4.18	1040	60.8	550	1950	58.5	1.68	1.68	1.06
E06	120	180	4.18	1040	72.1	550	1140	79.8	1.02	1.02	0.87
E07	80	120	4.18	1740	60.8	550	660	13.2	0.86	0.86	0.78
E08	80	120	4.18	1740	72.1	550	855	17.1	1.51	1.51	0.96
E09	100	200	4.18	1150	60.8	550	1310	78.6	1.23	1.23	1.00
E10	100	200	4.18	1150	72.1	550	1800	72	1.37	1.37	1.06
E11	80	160	4.18	2310	60.8	550	670	40.2	1.35	1.35	0.98
E12	80	160	4.18	2310	72.1	550	1020	30.6	1.61	1.61	1.00
Average									1.02	1.27	0.96
Coefficient of variation									0.23	0.19	0.08

Table 3 Analysis results for test data 3 (Liu, Gho, and Yuan 2003)

Specimen	B (mm)	H (mm)	t (mm)	L (mm)	f_c' (MPa)	f_y (MPa)	P_{test} (kN)	M_{test} (kN·m)	P_{test}/P_n or M_{test}/M_n		
									ACI 05	AISC 05	Authors
C1-1	98.2	100.3	4.18	300	60.8	550	1490	0	1.10	1.17	0.96
C1-2	100.6	101.5	4.18	300	60.8	550	1535	0	1.10	1.18	0.97
C2-1	101.1	101.2	4.18	300	72.1	550	1740	0	1.17	1.25	1.01
C2-2	100.4	100.7	4.18	300	72.1	550	1775	0	1.20	1.29	1.04
C3	181.2	182.8	4.18	540	60.8	550	3590	0	1.04	1.14	0.95
C4	180.4	181.8	4.18	540	72.1	550	4210	0	1.12	1.24	1.02
C5-1	80.1	120.7	4.18	360	60.8	550	1450	0	1.07	1.14	0.95
C5-2	80.6	119.3	4.18	360	60.8	550	1425	0	1.06	1.13	0.96
C6-1	80.6	119.6	4.18	360	72.1	550	1560	0	1.08	1.16	0.95
C6-2	80.6	120.5	4.18	360	72.1	550	1700	0	1.17	1.26	1.03
C7-1	121.5	179.7	4.18	540	60.8	550	2530	0	1.01	1.1	0.93
C7-2	120.5	181.4	4.18	540	60.8	550	NA	NA	-	-	-°°
C8-1	119.8	180.4	4.18	540	72.1	550	2970	0	1.10	1.2	1.01
C8-2	121.3	179.2	4.18	540	72.1	550	2590	0	0.95	1.04	0.88
C9-1	81.4	160.2	4.18	480	60.8	550	1710	0	0.99	1.06	0.91
C9-2	80.5	160.7	4.18	480	60.8	550	1820	0	1.06	1.13	0.96
C10-1	81.0	160.1	4.18	480	72.1	550	1880	0	1.02	1.1	0.93
C10-2	80.1	160.6	4.18	480	72.1	550	2100	0	1.14	1.23	1.04
C11-1	101.2	199.8	4.18	600	60.8	550	2350	0	0.98	1.06	0.92
C11-2	98.9	200.2	4.18	600	60.8	550	2380	0	1.00	1.08	0.94
C12-1	102.1	199.2	4.18	600	72.1	550	2900	0	1.11	1.21	1.04
C12-2	99.6	199.8	4.18	600	72.1	550	2800	0	1.09	1.18	1.01
Average									1.02	1.16	0.97
Coefficient of variation									0.23	0.06	0.05

Table 4 Analysis results for test data 4 (Lue, Liu, and Yen 2007)

Specimen	B (mm)	H (mm)	t (mm)	L (mm)	f_c' (MPa)	f_y (MPa)	P_{test} (kN)	M_{test} (kN·m)	P_{test}/P_n or M_{test}/M_n		
									ACI 05	AISC 05	Authors
C4 4-1-4	150	100	4.5	1855	29	380	1328.5	0	1.11	1.43	1.05
C9 6-1-6	150	100	4.5	1855	63	380	1722.3	0	1.06	1.46	1.00
C10 6-1-6	150	100	4.5	1855	70	380	1885.5	0	1.09	1.53	1.04
C12 6-1-6	150	100	4.5	1855	84	380	2089.8	0	1.1	1.58	1.08
Average									1.13	1.50	1.04
Coefficient of variation									0.08	0.05	0.03

Table 5 Analysis results for test data 5 (Liu 2005)

Specimen	B (mm)	H (mm)	t (mm)	L (mm)	f_c' (MPa)	f_y (MPa)	P_{test} (kN)	M_{test} (kN·m)	P_{test}/P_n or M_{test}/M_n		
									ACI 05	AISC 05	Authors
R1-1	120	120	4	360	60	495	1701	0	1.03	1.11	0.91
R1-2	120	120	4	360	60	495	1657	0	1	1.08	0.88
R2-1	100	150	4	450	60	495	1735	0	1.01	1.09	0.91
R2-2	100	150	4	450	60	495	1778	0	1.03	1.11	0.93
R3-1	90	180	4	540	60	495	1773	0	0.95	1.03	0.88
R3-2	90	180	4	540	60	495	1795	0	0.96	1.04	0.90
R4-1	130	130	4	390	60	495	2020	0	1.08	1.17	0.95
R4-2	130	130	4	390	60	495	2018	0	1.08	1.17	0.95
R5-1	110	160	4	480	60	495	1982	0	1.02	1.1	0.93
R5-2	110	160	4	480	60	495	1923	0	0.99	1.07	0.90
R6-1	100	190	4	570	60	495	2049	0	0.97	1.06	0.92
R6-2	100	190	4	570	60	495	2124	0	1.01	1.09	0.95
R7-1	106	106	4	320	89	495	1749	0	1.06	1.16	0.93
R7-2	106	106	4	320	89	495	1824	0	1.11	1.21	0.97
R8-1	90	130	4	390	89	495	1752	0	1.02	1.12	0.92
R8-2	90	130	4	390	89	495	1806	0	1.05	1.15	0.95
R9-1	80	160	4	480	89	495	1878	0	1	1.09	0.93
R9-2	80	160	4	480	89	495	1858	0	0.99	1.08	0.93
R10-1	140	140	4	420	89	495	2752	0	1.05	1.17	0.94
R10-2	140	140	4	420	89	495	2828	0	1.08	1.2	0.98
R11-1	125	160	4	480	89	495	2580	0	0.97	1.07	0.90
R11-2	125	160	4	480	89	495	2674	0	1	1.11	0.93
Average									1.02	1.11	0.93
Coefficient of variation									0.04	0.05	0.03

Liu (2004) performed the experimental study on the behavior of 12 high strength rectangular CFT columns subjected to eccentric loading. The axial load was slowly applied to the specimen by careful manipulation of the loading and unloading values. During the test, the longitudinal and the transverse strains as well as the in-plane and out-plane deflections of the specimen were recorded at a load increment of 50 kN. The out-plane deflection of the specimen was less than 1 mm, thus the

Table 6 Analysis results for test data 6 (Liu 2006)

Specimen	B (mm)	H (mm)	t (mm)	L (mm)	f_c' (MPa)	f_y (MPa)	P_{test} (kN)	M_{test} (kN·m)	P_{test}/P_n or M_{test}/M_n		
									ACI 05	AISC 05	Authors
S1	120	120	4	360	60	495	1294	19.4	1.11	1.11	0.91
S2	120	120	4	360	60	495	1125	28.1	0.96	0.96	0.93
S3	120	120	4	360	60	495	949	28.5	0.97	0.97	0.84
S4	120	120	4	360	60	495	810	36.5	1.1	1.1	0.85
S5	100	150	4	450	60	495	1422	21.3	1.18	1.18	0.94
S6	100	150	4	450	60	495	1190	35.7	1.23	1.23	0.95
S7	100	150	4	450	60	495	964	43.4	1.17	1.17	0.93
S8	100	150	4	450	60	495	763	45.8	1.05	1.05	0.85
S9	90	180	4	540	60	495	1491	29.8	1.17	1.17	0.97
S10	90	180	4	540	60	495	1319	39.6	1.14	1.14	0.95
S11	90	180	4	540	60	495	1208	48.3	1.21	1.21	0.97
S12	90	180	4	540	60	495	1051	52.6	1.14	1.14	0.93
S13	130	130	4	390	60	495	1472	22.1	1.04	1.04	0.90
S14	130	130	4	390	60	495	1305	32.6	1.17	1.17	0.92
S15	130	130	4	390	60	495	1022	40.9	1.1	1.1	0.88
S16	130	130	4	390	60	495	789	43.4	0.99	0.99	0.80
L1	100	150	4	2600	60	495	1130	17.0	1.99	1.99	0.98
L2	100	150	4	2600	60	495	884	26.5	1.55	1.55	0.99
L3	100	150	4	2600	60	495	711	32.0	1.31	1.31	0.96
L4	100	150	4	2600	60	495	617	37.0	1.28	1.28	0.98
Average									1.19	1.19	0.92
Coefficient of variation									0.19	0.19	0.06

specimen was conformed to be under compression combined with uniaxial bending. For specimens with slenderness ratio of 20, crushing of concrete and local buckling of steel tube were observed. For specimens with slenderness ratio of 50, the failure loads were reached followed by local buckling of steel tube at the mod height of the specimen.

Liu, Gho, and Yuan (2003) investigated the ultimate capacity of 22 high-strength rectangular CFT columns with cross-sectional aspect ratio of 1.0, 1.5, and 2.0. The main parameters of the test specimens are the strengths of concrete and steel, cross-sectional aspect ratio, and volumetric steel-to-concrete ratio. The two horizontal flat plates welded at both ends of the specimen were to ensure that the steel hollow section and the core concrete were simultaneously loaded during the test. In addition, local yielding at both ends of the steel hollow section could be avoided. The specimens were tested to failure under axial concentric loading. The failure mechanism was identified as the material yielding of steel hollow sections and the crushing of core concrete.

Lue, Liu, and Yen (2007) tested twenty four 1855 mm long rectangular CFT columns of $150\times100\times4.5$ mm. The specimens were divided into four groups, and the sections in each group are filled with approximate concrete strength f_c' of 29, 63, 70, and 84 MPa, respectively. Two bearing plates ($340\times340\times20$ mm) were welded at the top and bottom ends of each specimen with eight spot-welded stiffeners to provide the rigidity plane at the ends of the specimen when the rotation occurs at the onset of buckling. Most of the specimens with normal-strength concrete failed in global buckling. Pure local buckling cases were not detected, and the failure modes are either global buckling or mixed global-local buckling.

Liu (2005) tested 22 high-strength rectangular CFT columns under concentric loading. The test variables include the material strengths (f_c' = 60 and 89 MPa), cross-sectional aspect ratio (1.0-2.0) and volumetric steel-to-concrete ratio (0.13-0.17). Concrete was then vertically cast into the steel hollow section in three layers. Each layer of concrete was compacted by a poker vibrator. Then the concrete was cured inside the steel hollow section with top open to the air for two weeks until a 10-mm-thick flat plate was welded to the top to form a complete specimen. It was reported that the ductility enhancement was significant due to the confinement by the steel section.

Liu (2006) tested 16 short and 4 slender CFT columns under eccentric loading about major axis. The CFT specimen was cured in the laboratory with top open to the air for 14 days for the concrete to set. High-strength cement mortar was subsequently infilled to flush the concrete core with the steel tube. Finally, the top cap plate was welded to form a complete specimen. It was observed that the short CFT columns with load eccentricity ratio with 0.10-0.42 cannot fully develop material plasticity at the failure load. Hence, plastic assumptions will not be suitable for the numerical analysis on them. The four slender columns performed in a much similar failure mode to each other, and the failure was characterized as overall buckling.

Fig. 5 shows that the predictions by the ACI 318-05 and AISC are generally conservative with

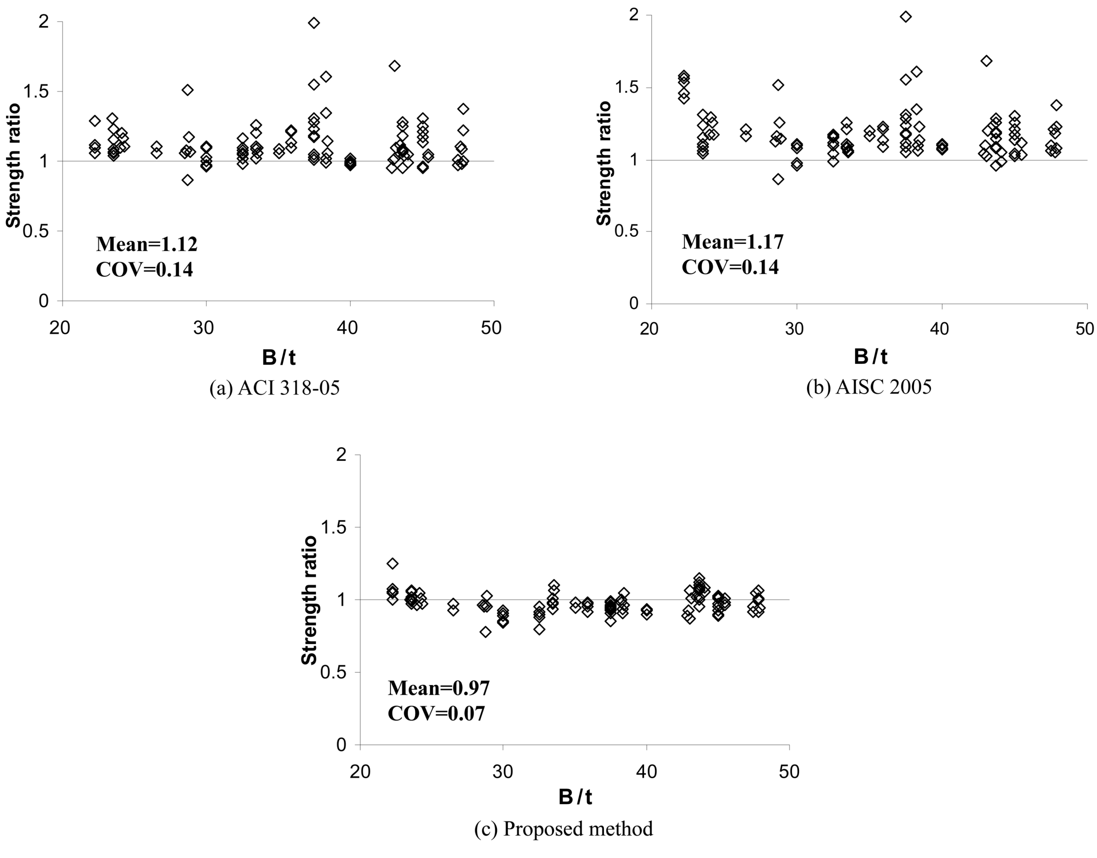

Fig. 5 Ratio of measured-to-calculated strengths by different methods

mean values of 1.12 and 1.17, respectively, and coefficients of variation of 0.14 for both methods. For slender columns, the predictions by the two code methods are more conservative and scattered with mean values of 1.30 and 1.43, and COVs of 0.21 and 0.18, respectively. The main cause of this scatter may be the difficulty in evaluating the geometric second-order effects for slender columns subjected to axial load and bending moments using the simplified equations in the code practices. The calculated capacities by the proposed method are significantly accurate with little scatter or trends for rectangular CFT columns over a wide range in concrete strengths, various combinations of loading, and various width-to-thickness ratios (B/t) and column lengths. It would be useful to expand this evaluation to include even more test data and other code provisions such as Eurocode 4 and Architectural Institute of Japan code.

The 102 specimens are short columns in which the slenderness effects can be neglected when the ACI code is applied for column design. The other 15 specimens are slender columns, therefore, the second-order effects must be considered by increasing the moment. For a slender column, buckling may occur when all fibers of the cross-section are still elastic. Thus, the Euler load will govern the load-carrying capacity of the column. For a short column, material yielding of the fibers in the cross-section usually occurs before buckling takes place, so the yielding force of the section will govern the limit state of the column. For a medium length column, some of the fibers of the cross-section may yield while some fibers still remain elastic. In this case, the failure may be more accurately described as combined buckling of the column and material yielding of the section.

To investigate the capability of the proposed method for capturing the elastic buckling or critical load, five end-restrained steel columns with different end conditions as shown in Fig. 6 are analyzed. The analysis of steel columns concentrates on the buckling behavior as a result of geometric second-order effects while the material is in the range of linear elastic. The columns are subjected to small end moments or lateral end forces in addition to axial compressive force to initiate the desired buckling mode. The exact value of Euler load or critical load can be obtained from the effective length factor that is dependent on the support condition of the column. The effective length factors for the pinned-ended, one end fixed and one end free, one end fixed and one end hinged, one end fixed and one end guided, and one end hinged and one end guided columns are 1.0, 2.0, 0.7, 2.0, and 1.0, respectively.

From Fig. 7 to Fig. 11, the theoretical critical loads are compared collectively with the results

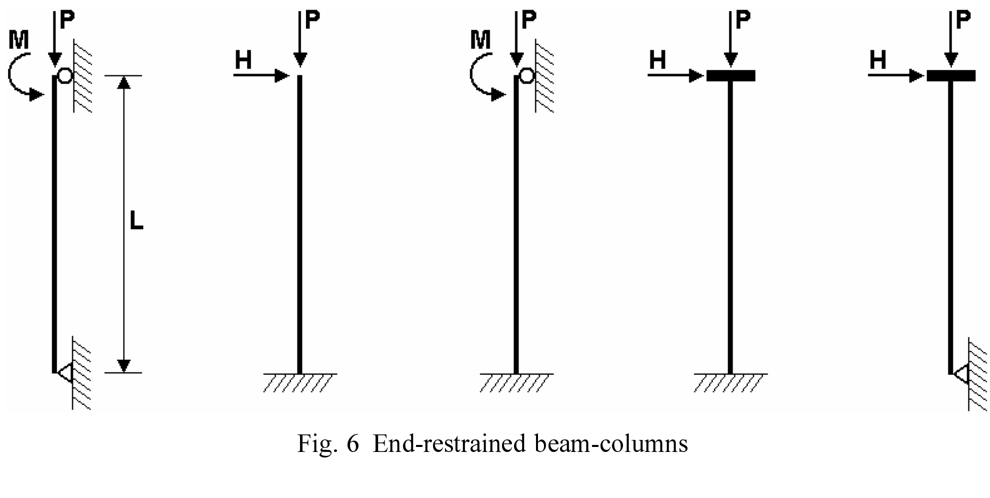

Fig. 6 End-restrained beam-columns

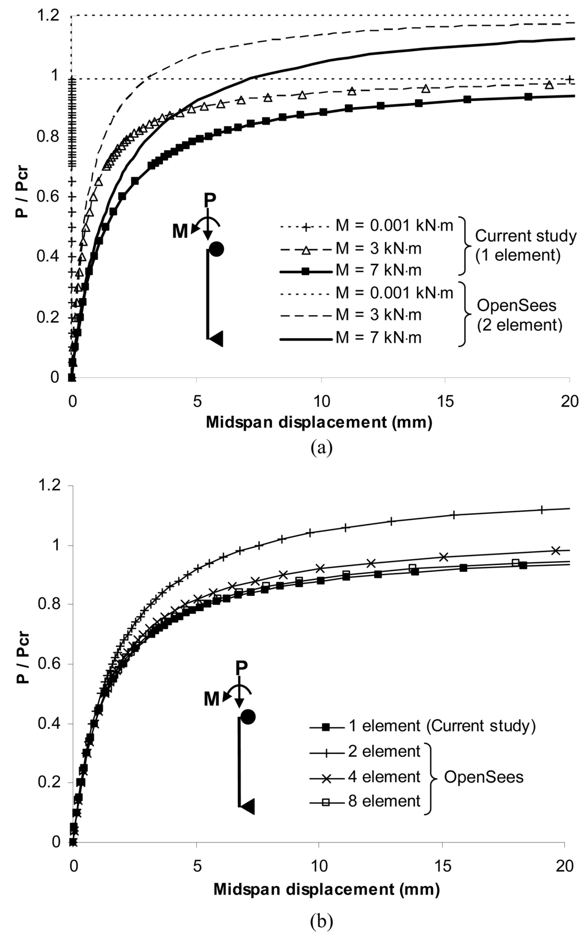

Fig. 7 Pinned-ended column

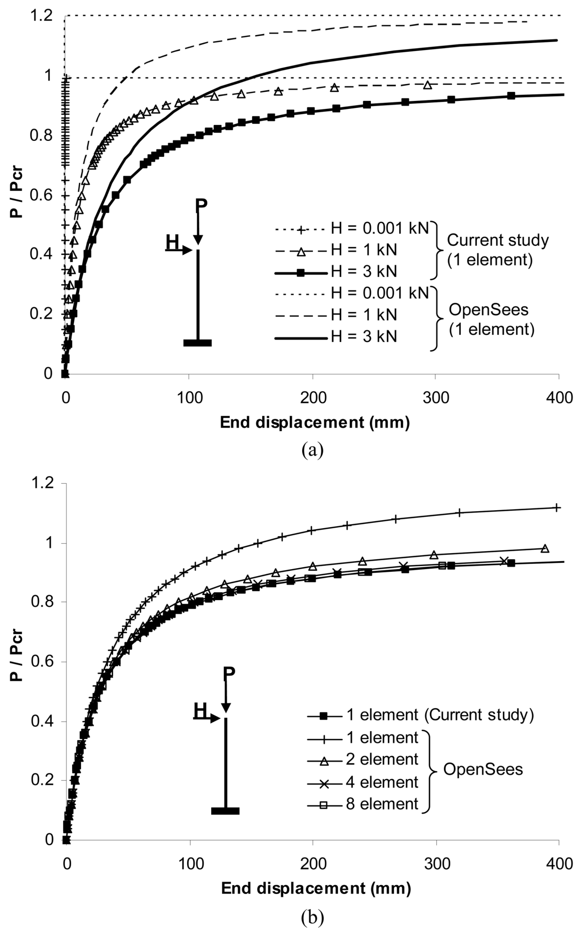

Fig. 8 One end fixed and one end free column

obtained from the proposed method and OpenSees (2008). The buckling load is not given directly in the nonlinear finite element analysis, but rather a complete load-deformation response is obtained from the two methods. Fig. 7(a) to Fig. 11(a) show the relationships between compressive axial forces and lateral displacements according to the different end moments or lateral end forces. The "nonlinearBeamColumn" element object based on a force-based formulation with five integration points along the element is used in the OpenSees analysis. The proposed method accurately calculates the elastic buckling loads for the various beam-columns with different end conditions even using one beam-column element. However, the OpenSees overestimates the critical loads by 34% for one end hinged and one end fixed member, and by 20% for all other cases. Fig. 7(b) to Fig. 11(b) show the load-displacement responses by the proposed method and OpenSees with respect to the number of elements in OpenSees analysis model. As the number of elements increases, the OpenSees result becomes closer to those of the proposed method, and using eight beam-column elements in the analysis by OpenSees gives very similar results to the proposed method.

A three-dimensional CFT portal frame as shown in Fig. 12 is analyzed by the proposed method

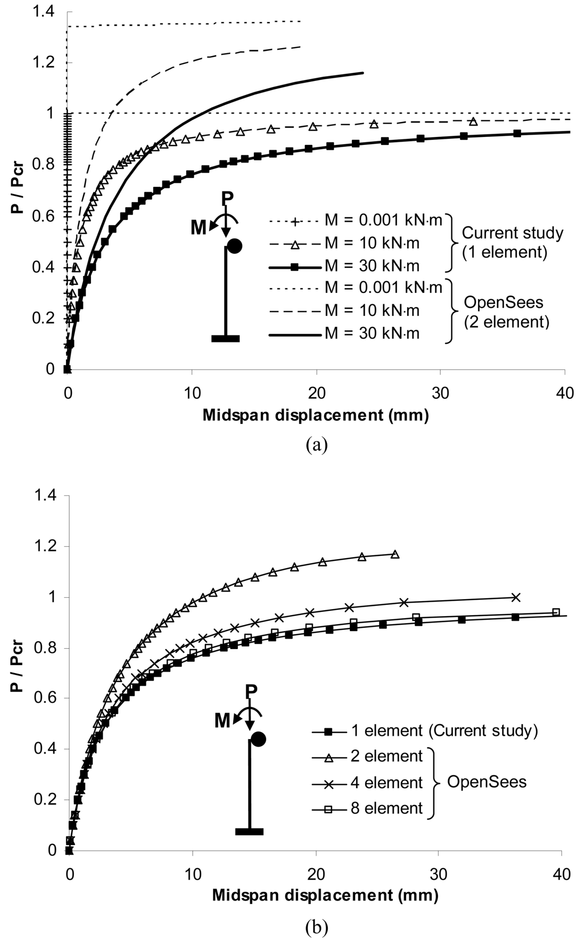

Fig. 9 One end fixed and one end hinged column

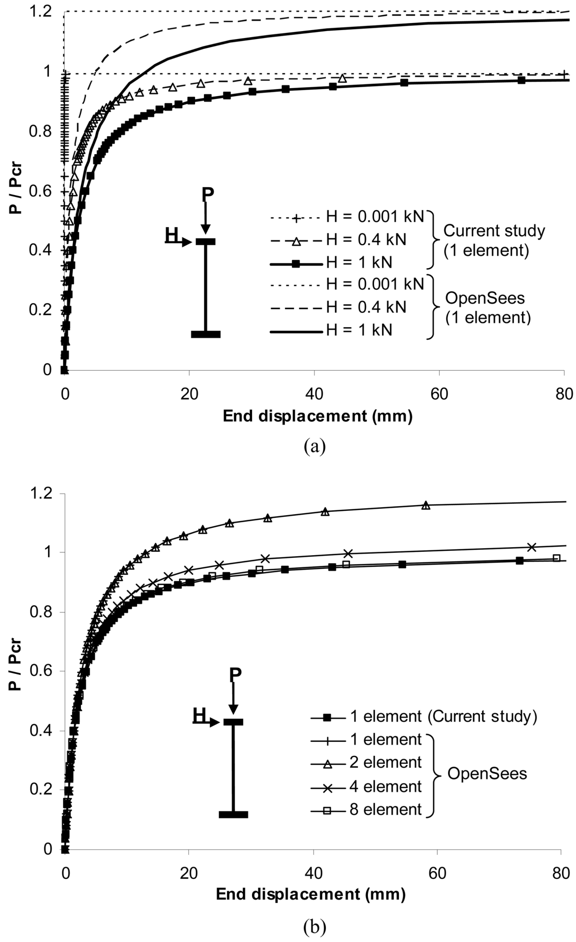

Fig. 10 One end fixed and one end guided column

and OpenSees. The section of each integration point is divided by 100 rectangular fiber segments. The frame structure is subjected to horizontal force at node 10 to impose the torsion as well as gravity loads. It is assumed that steel tube and concrete are fully constrained, and the local buckling can be avoided by using the CFT section with B/t ratio within the range specified in the AISC specification (2005). The "nonlinearBeamColumn" element object based on a force-based formulation with five integration points along the element is used, and each member is modeled by ten beam-column elements in the OpenSees. Fig. 13 shows the deformed shape obtained from the proposed method in exaggerated scale. The load-displacement responses for the direction of x-axis at node 5 and node 10 are shown in Fig. 14 with respect to the number of elements. The response for the direction of z-axis at node 10 is shown in Fig. 15. The responses of the proposed method using one and four elements are in good agreement with those obtained from the four nonlinear beam-column elements of OpenSees, as shown in Fig. 14 and Fig. 15. The critical load calculated by using one nonlinear beam-column element of OpenSees is about 10% higher than that obtained by four elements of the same element object. The stresses of concrete and steel fibers still remain elastic. According to the analysis results, a good accuracy is obtained by the proposed method with

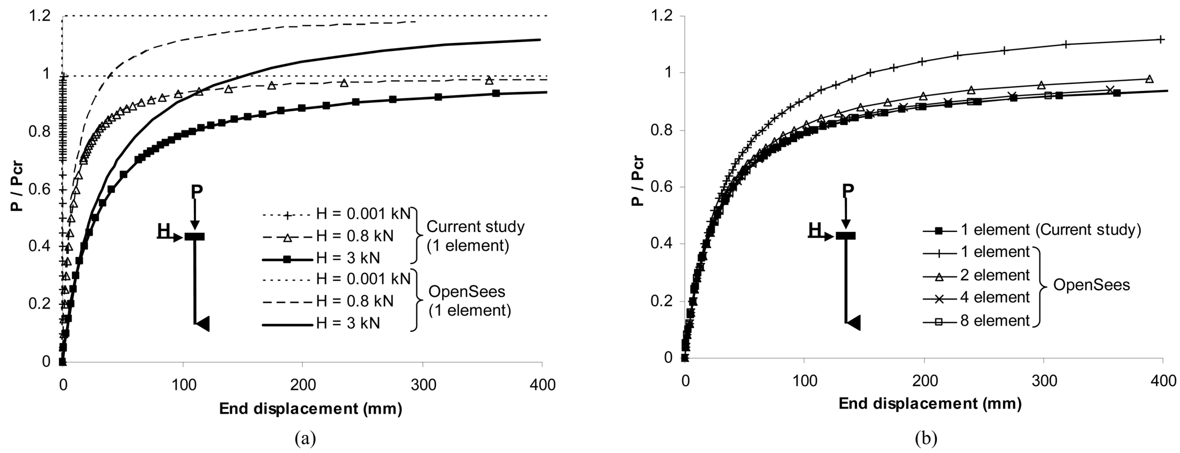

Fig. 11 One end hinged and one end guided column

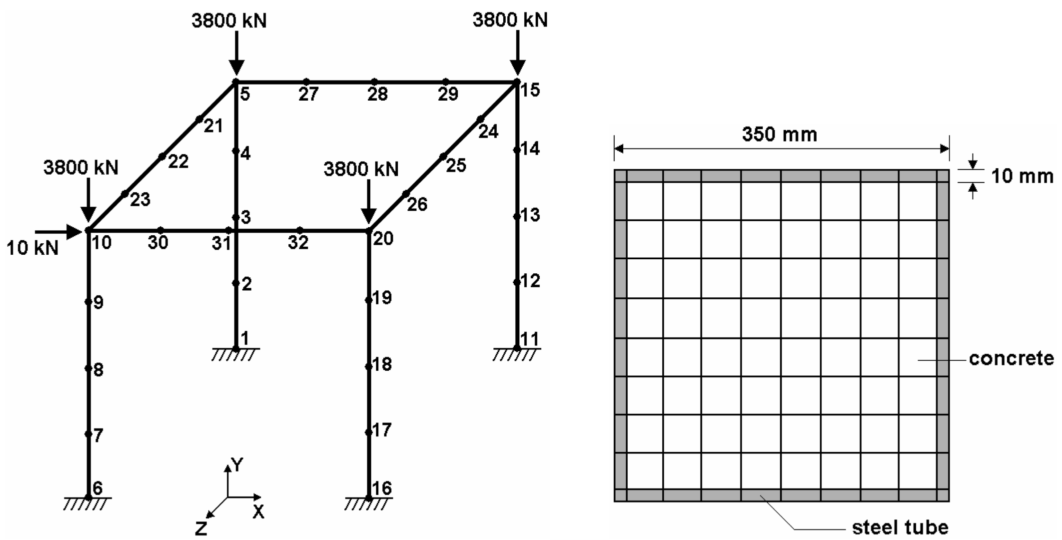

Fig. 12 3-dimensional CFT frame structure

reduced computational cost. Present work can be considered as a progressive contribution for engineering design and performance evaluation (Chen 2008).

6. Conclusions

In this study, a flexibility-based finite element method has been developed for nonlinear inelastic analysis of steel-concrete composite frames in the context of a standard finite element analysis program. From the results of this study, the following conclusions can be made:

1) ACI 318-05 and AISC give reasonably conservative estimates for short CFT columns. However, for slender columns, the predictions by the two code methods become more

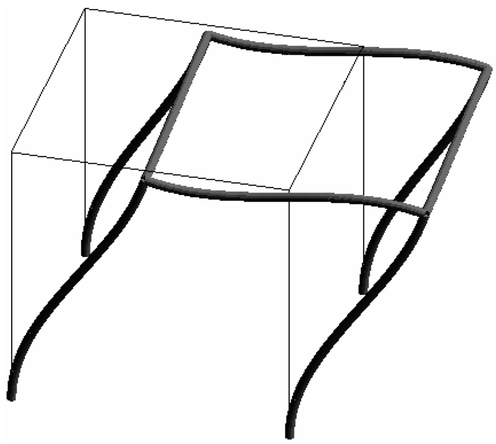

Fig. 13 Deformed shape of the 3-D frame

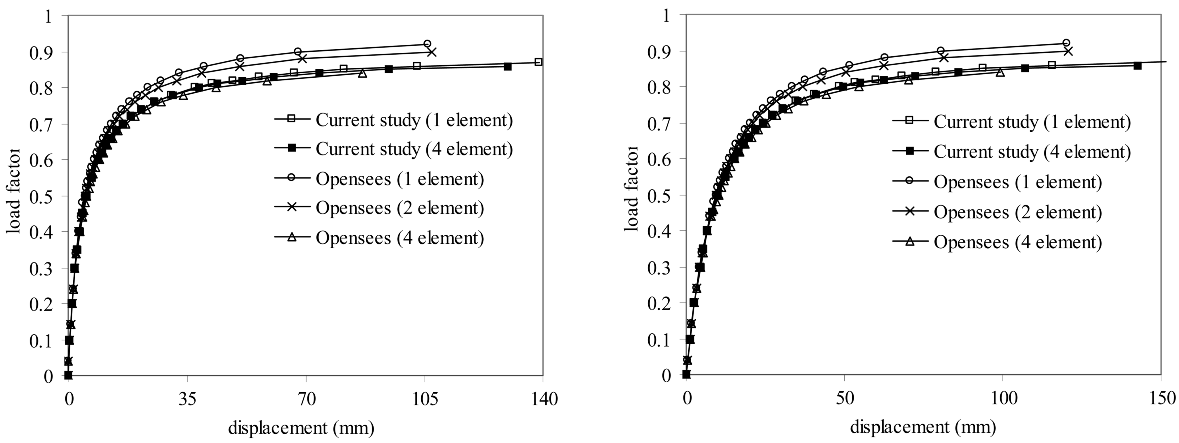

(a) node 5 (b) node 10

Fig. 14 Load-displacement relationships for the direction of x-axis

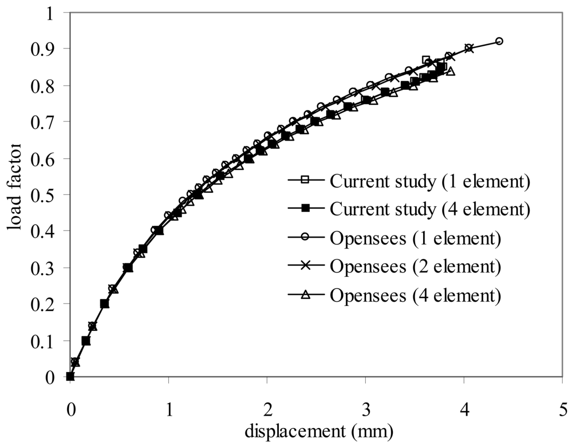

Fig. 15 Load-displacement relationships at node 10 for the direction of z-axis

conservative and scattered due to the difficulty in evaluating the geometric second-order effects for slender columns subjected to axial load and bending moments using the simplified equations in the code practices.

2) The proposed method can account for the interaction between the bending moment and the axial force in a rational way using the stability functions obtained from the exact buckling solution of a beam-column. Thus, using only one element per a physical member provides most accurate strength predictions for the 116 rectangular CFT columns tested to failure.
3) The proposed method accurately capture the elastic buckling or critical loads for the five end-restrained beam-columns with different end conditions even using one beam-column element. The analysis results using one element by the proposed method for the three-dimensional CFT frame structure are in good agreement with those obtained from the four nonlinear beam-column elements of OpenSees.
4) Good accuracy can be obtained by the proposed method with reduced computational cost. The method can provide valuable insight into the design and behavior of CFT beam-columns.

Acknowledgements

This paper is a part of the result from the “Standardization of Construction Specifications and Design Criteria based on Performance(’06~’11)”, the “Construction & Transportation R&D Policy and Infrastructure Project”.

References

ACI 318-05 (2005), Building code requirements for reinforced concrete (ACI 318-05) and Commentary (ACI 318R-05). American Concrete Institute.

AIJ (1997), Recommendations for design and construction of concrete filled steel tubular structures. Architectural Institute of Japan.

AISC (2005), Specification for structural steel buildings. American Institute of Steel Construction.

Alemdar, B.N. and White, D.W. (2005), “Displacement, flexibility, and mixed beam-column finite element formulations for distributed plasticity analysis”, *J. Struct. Eng. ASCE*, **131**(12), 1811-1819.

Ayoub, A. (2003), “Mixed formulation of nonlinear beam on foundation elements”, Comput. Struct., **81**(7), 411-421.

Ayoub, A. and Filippou, F.C. (2000), “Mixed formulation of nonlinear steel-concrete composite beam element”, *J Struct. Eng. ASCE*, **126**(3), 371-381.

Chen, W.F. (2008), “Structural engineering: Seeing the big picture”, *KSCE J. Civil Eng.*, **12**(1), 25-29.

Chen, W.F. and Lui, E.M. (1987), “Structural stability: theory and implementation”, Elsevier, New York.

Ciampi, V. and Carlesimo, L. (1986), “A nonlinear beam element for seismic analysis of structures”, *Proc. 8th Euro. Conf. Earthq. Eng.*, Lisbon, Portugal, 73-80.

Eurocode 4, ENV 1994-1-1 (2004), “Design of composite steel and concrete structures, Part 1.1, General rules and rules for building”, *Commission of European Communities*.

Hjelmstad, K.D. (1997), “Fundamentals for structural mechanics”, Prentice Hall.

Hjelmstad, K.D. and Taciroglu, E. (2002), “Mixed methods and flexibility approaches for nonlinear frame analysis”, *J. Constr. Steel Res.*, **58**(5-8), 967-993.

Kim, S.E., Uang, C.M., Choi, S.H., and An, K.Y. (2006), “Practical advanced analysis of steel frames considering lateral-torsional buckling”, *Thin Wall Struct.*, **44**(7), 709-720.

Liu, D. (2004), “Behaviour of high strength rectangular concrete-filled steel hollow section columns under

eccentric loading", *Thin Wall Struct.*, **42**(12), 1631-1644.
Liu, D. (2005), "Tests on high-strength rectangular concrete-filled steel hollow section stub columns", *J. Constr. Steel Res.*, **61**(7), 902-911.
Liu, D. (2006), "Behaviour of eccentrically loaded high-strength rectangular concrete-filled steel tubular columns", *J. Constr. Steel Res.*, **62**(8), 839-846.
Liu, D., Gho, W.M., and Yuan, J. (2003), "Ultimate capacity of high-strength rectangular concrete-filled steel hollow section stub columns", *J. Constr. Steel Res.*, **59**(12), 1499-1515.
Lue, D.M., Liu, J.L., and Yen, T. (2007), "Experimental study on rectangular CFT columns with high-strength concrete", *J. Constr. Steel Res.*, **63**(1), 37-44.
Mander, J.B., Priestly, J.N., and Park, R. (1988), "Theoretical stress–strain model for confined concrete", *J. Struct. Eng. ASCE*, **114**(8), 1804-1826.
OpenSees user command-language manual (2008), *Pacific Earthquake Engineering Research Center*, Univ. of California, Berkeley.
Popovics, S. (1973), "A numerical approach to the complete stress–strain curves for concrete", *Cement Concrete Res.*, **3**(5), 583-599.
Spacone, E., Ciampi, V., and Filippou, F.C. (1996), "Mixed formulation of nonlinear beam finite element", *Comput. Struct.*, **58**(1), 71-83.
Spacone, E., Filippou, F.C., and Taucer, F.F. (1996), "Fibre beam column model for nonlinear analysis of R/C frames: Part I. formulation", *Earthq. Eng. Struct. D*, **25**(7), 711-725.
Susantha, K.A.S., Ge, H., and Usami, T. (2001), "Uniaxial-stress-strain relationship of concrete confined by various shaped steel tubes", *Eng. Struct.*, **23**(10), 1331-1347.
Taucer, F.F., Spacone, E., and Filippou, F.C. (1991), "A fiber beam-column element for seismic response analysis of reinforced concrete structures", Report No. EERC 91-17, *Earthquake Engineering Research Center*, Univ. of California, Berkeley.
Tomii, M. and Sakino, K. (1979), "Experimental studies on the ultimate moment of concrete filled square steel tubular beam-columns", *T. Arch. Inst. JPN*, **275**, 55-63.
Tort, C. and Hajjar, J.F. (2004), "Damage assessment of rectangular concrete-filled steel tubes for performance-based design", *Earthq. Spectra*, **20**(4), 1317-1348.